Proceedings of The 2016 IEEE International
Conference on Real-time Computing and Robotics
June 6-9, 2016, Angkor Wat, Cambodia

GPU-based Heuristic Escape for Outdoor Large Scale Registration*

Peng Yin*, Feng Gu, Decai Li, Yuqing He*, Liying Yang and Jianda Han*

***Abstract*—heterogeneous robot introduce a higher perception ability than single type robots in outdoor environments. One key problem is to making the 3D environmental model from the cooperated robots in real time, especially in the unstructured environment. Based on our previous work on outdoor environment registration method, in this paper, we introduce a GPU based Enhanced ICP method for large-scale heterogeneous robot registration. First, we combine the GPU-based nearest neighbor search in the traditional ICP framework. Second, we proposed a measurement and estimation model for the local minima problem. Third, we proposed a GPU-based heuristic escape method to generate the escaping transformation in real time. Experiments involving one unmanned aerial vehicle and one unmanned surface vehicle were conducted to verify the proposed technique. The experimental results were compared with those of normal ICP registration algorithms to demonstrate the performance of the proposed method.**

I. INTRODUCTION

Due to the performance complementarity, heterogeneous multiple robot systems, composed of aerial unmanned vehicle (UAV), unmanned ground vehicle (UGV) and unmanned surface vehicle (USV), present much stronger capabilities in the aspects of both environmental perception and behavior decision making than both single robot system and traditional homogeneous multiple mobile robot systems. However, it also introduces some grand challenges to achieve effective coordination for multiple heterogeneous robots. One of the key challenges is about how to make alignments between different environmental information obtained from different robots, i.e., the large scene 3D model registration. Besides the difference in the aspects of viewpoint and resolution level, it is hard to find the structured reference in the dense outdoor scenes.

Iterative closest point (ICP)[1] method has been widely used in 2D/3D model registration problem. Traditional ICP method is Point-to-Point based, which define the distance based on the paired points, but it presents bad performance without a good initial estimation. Since it is firstly supposed, there have been many different variants of traditional ICP algorithms. Point-to-Plane [2] ICP can be used to improve the performance by taking advantage of the surface normal information to improve the searching efficiency. Recently, Alsksandr [3] introduced a Plane-to-Plane based ICP algorithm which use surface structure to measure the distance. This method has been proved to be more robust with respect to initial transformation error and maintain the real time performance of standard-ICP method. There are also some kinds of ICP algorithms which take advantage of Multi-Resolution scheme. Jost [4] adopt multi-resolution scheme to accelerate the registration procedure. When used in large scale model registration, one of the important disadvantages of most ICP algorithms is the problem of local minima. Thus, for most ICP methods, a good enough initialized value is necessary to ensure the final high precision registration, otherwise, the final solution may be far away from the true global optimal solution and result in failure of registration method. Most recent, Yang [5] proposed a so called global optimal ICP (Go-ICP) to solve the local minima problem. This method combined the ICP framework with a branch-and-bound (BnB) scheme which searches the 3D motion space SE (3) efficiently, and could guarantee an exactly global optimal in practice. But this method is not practical for the large scale model matching problem, because it requires the initial translation error to be small. In our previous work [6], we introduce an enhanced-ICP method, which could predict the local minima problem by using an Early Warning Mechanism and escape from the local minima by using a heuristic escaping scheme. But the heuristic escaping scheme is very time consuming in the real application, this is because the desired escaping direction is estimated by sampling form different potential transformations.

In the recent years, with the development of Graphical Process Unit (GPU), many researchers has transform the traditional serial program into the parallel ones. Grabner [7] introduce an GPU based image registration method for CT image. Qiu [8] applied a GPU based near neighbor search in the 3D registration problem, and the speed up gain is 88 times compare to a sequential CPU implementation. In [9], the author use a GPU-based back projection to accelerate the real time video and LiDAR registration procedure. Liu [10] introduce a GPU based Normal Estimation method for pointcloud.

In this paper, we proposed a GPU based enhanced-ICP method for the large scale registration problem. The main contribution of this paper is threefold. First, we combine the GPU-based nearest neighbor search in the traditional ICP framework. Second, we proposed a measurement and estimation model for the local minima problem. Third, we proposed a GPU-based heuristic escape method to generate the escaping transformation in real time. The remainder of this paper is organized as follows: we describe the multi-resolution ICP and the GPU structure in section 2. In section 3, we expand the detail of the proposed method. The experiment and analysis is discussed in section 4. Finally we discuss future work in section 5.

*Research supported by the State Key Program of National Natural Science of China (Grant No. 61473282, 61433016, 61305121, 61503369).

Peng Yin is with the State Key Laboratory of Robotics, Shenyang Institute of Automation, Chinese Academy of Sciences, Shenyang 110016, University of Chinese Academy of Sciences, Beijing 100049, Email: yinpeng@sia.cn.

Feng Gu, Decai Li, Yuqing He, Liying Yang and Jianda Han are all with the State Key Laboratory of Robotics, Shenyang Institute of Automation, Chinese Academy of Sciences, Shenyang 110016, China. Email: fenggu, lidecai, heyuqing yangliying and jdhan@sia.cn.

978-1-4673-8959-4/16/$31.00 © 2016 IEEE

II. PRELIMINARIES

In this section, we first derive the multi-resolution ICP method and then recall the basic particle filter method.

A. Multi-Resolution ICP

The model point cloud $Q \in \{R^M\}$ has M points and the data point cloud $P \in \{R^N\}$ has N points, without losing generality, we assume that $M > N$, the basic registration method is to find the sub-point sets $\{q_i\}^N_{i=1}$ which is pair to the data point cloud P. To solve the problem, ICP based method gives the below equation

$$\begin{aligned} &\min_T(\sum_i^N \| (T\,\mathrm{p}_i - q_i \|^2) \\ &T = \begin{bmatrix} R & t \\ 0 & 1 \end{bmatrix} \\ &\text{s.t.} \quad R^T R = I, \det(R) = 1 \end{aligned} \tag{1}$$

where $T \in T^{4\times4}$ is the combination of rotation matrix R and translation vector t. That is, the registration problem of two 3D models has been converted into an optimization problem.

The multi-resolution has been spread used in computer vision, Jost [11] first introduce such scheme in 3D object registration method. Assume the point number of two 3D models are N and M, the computational complexity for normal ICP [12] method is $O(MN)$; with a kd-tree structure, the complexity could be converted down to $O(M\log N)$ [13] [14]; if we reduce the data size of both data and model point cloud by a factor n, here we assume $N>>n$, then the speed up gain compare to the single kd-tree enhanced ICP could be estimated by

$$\begin{aligned} Gain &= O(M\log N) / O(\frac{M}{n}\log\frac{N}{n}) \\ &= \mathrm{O}(n\frac{\log N}{\log N - \log n}) > \mathrm{O}(n) \end{aligned} . \tag{2}$$

The computational complex could decrease at least n times. Furthermore, if the registration process is applied on multi-resolution scheme, and set t_i as the iteration times for the ith resolution level. Then the corresponding computational complexity of the multi-resolution registration C_{multi} could be denoted by

$$C_{multi} = \sum_{i=0}^{k} \mathrm{t}_i C_{Fi} = \sum_{i=0}^{k} t_i \frac{\mathrm{M}}{n^i} \cdot O(\log N - \log n^i) \tag{3}$$

where C_{Fi} is the computational complexity of the standard Kd-tree ICP with resolution for grid size i.

In our multi-resolution registration, we set the registration times the iteration times is negative correlation with the resolution level. That is to say the registration times must satisfy the following restriction

$$t_0 \le t_1 \le t_2 \le \ldots \le t_k \tag{4}$$

Thus the computation gain between standard ICP and multi-resolution ICP is

$$\begin{aligned} Gain_{sum} &= \frac{C_{const}}{C_{multi}} = \frac{O(M\log N)\cdot t_m}{\sum_{i=1}^{k} t_i \frac{\mathrm{M}}{2^i}\cdot O(\log N - \log 2^i)} \\ &\approx \frac{t_m}{t_0 + \frac{t_1}{2} + \ldots + \frac{t_k}{2^{k-1}}} \ge \frac{t_m}{t_0 + \frac{t_0}{2} + \ldots + \frac{t_0}{2^{k-1}}} \approx \frac{t_m}{2t_0} \end{aligned} \tag{5}$$

where C_{const} is Standard Kd-tree ICP with high resolution, and t_m is the required times loop to meet the same registration accuracy on the constant high resolution level. Even though the speed up gain $Gain_{sum}$ may be variant according to the property of the scenes, in our experiment test, this parameters could be ranged from 10~30 times. Besides the accelerate property, coarse-to-fine registration process also improve the robustness to the local optimal, we have shown this property in our previous work [6].

B. GPU framework

GPUs are designed for rendering 3D-graphics in games and applications, but since the first shader-capable were launched with GeForce 3 series of cards, GPUs have been applied for more and more parallel communication cases. In 2006, NVIDIA launched their Compute unified device architecture (CUDA) [15] to easy adoption of GPU technology for general purpose of computation. CUDA integrates the vertex shader and the pixel shader into a unified processor called streaming processor (SP). 8 SPs form a cluster called streaming multiprocessor (SM). The execution model of CUDA is characterized as *single instruction multiple thread* (SIMT). A warp of 32 threads share with the same instruction fetching unit, so only the same type of instructions within a warp can be parallelized perfectly. Otherwise, different instructions or divergent branching within a warp may lead to inefficient serial execution.

The memory hierarchy of an SM can be classified as four types: 1) an abundant set of registers per SP, 2) a 16-banke shared memory with limited entries for all SPs within an SM, 3) read-only caches mapped to texture memory and constant memory, and 4) a global on-device memory which can be written and read by all SMs. The accessing time of four types of memory varies greatly due to their hardware nature. The global memory are slower than other types of memory by about 100 times. Without optimization on the data locality or reduction of the global memory accessing time first, other improvements would be rather insignificant. Therefore, an efficient implementation on CUDA must provide proper solutions to these issues.

III. NEW PROPOSED REGISTRATION ALGORITHM

Figure 1 shows a flowchart of our GPU based registration method. After the preprocessing step and multi-resolution maps extraction, the registration method is combined with the following three steps: GPU-based ICP, Early Warning Mechanism and GPU-based Heuristic Escaping.

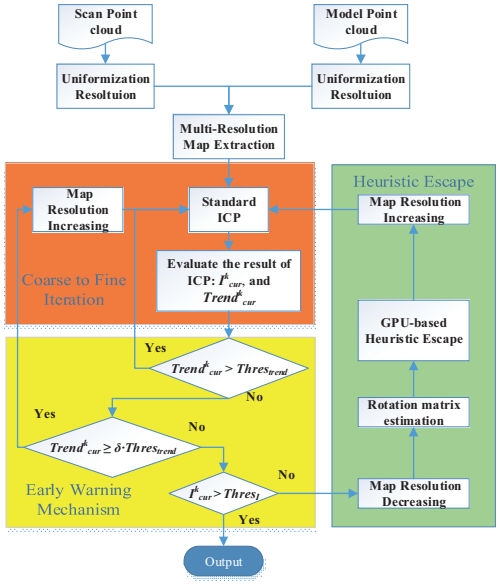

Figure 1. Pipe flow of the enhanced ICP: Coarse-to-Fine Iteration works as a Multi-Resolution ICP registration step; Early Warning Mechanism is introduced to estimate the potential local optima; Heuristic Escaping help the data point cloud escape from the current local optimal by estimating the potential optimal transformation.

A. Measurement and estimate

Because each particle represent a potential original position of data point cloud, so we use the registration result to weight each particles. After transforming the data point cloud P according to the particle i as point cloud P^k_i, where k is the current resolution level and original points of P^k_i is u^i_{t-1}, the Standard ICP method is used here to make the alignment. According to Eq. (1), the optimal transformation matrix T_{opt} is evaluated by L2 norm based gradient decent method. As shown in the Figure 2, the pointcloud at particle i is transformed into a now point cloud $n\_P^k_i$, where the new original point is $\hat{u}^i_{t-1}$, and the translation vector could be given as

$$v^i_{t-1} = \hat{u}^i_{t-1} - u^i_{t-1} \tag{6}$$

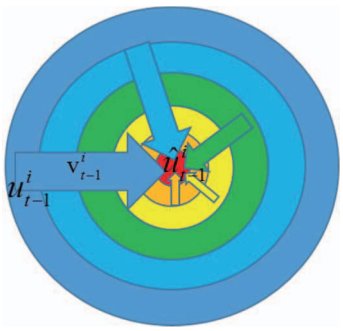

Figure 2. Stochastic Measurement Update

To measure the registration accuracy we use the registration index w^k_i which is defined in our previous work [6] for the current resolution level k and particle i

$$w^k_i = \exp(1/D_k)$$
$$D_k = \left(\sum_{j=1}^{N_p} \| \hat{q}^k_j - T_{opt}\hat{p}^k_j \|^2\right) \tag{7}$$

where D_k is the sum of the Euclidean distances between the scan point $\hat{p}^k_j$ and its nearest model point $\hat{q}^k_j$. The weighting of the particle i is then valued by the registration index.

The important particle extraction is the key step not only for resampling mechanism of particle filter, but also for our proposed map updater model in the next section. The main purpose of the map updater to reduce the sample scope when the map grid resolution grown higher by estimating the important particles' position and convergence efficiency. Here we define the tendency index $Trend^k_i$ to describe the convergence tendency

$$Trend^k_i = \frac{(w^k_i - w\_pre^k_i)}{Time^k_i \cdot Grid^k} \tag{8}$$

where $I\_pre^k_{pre}$ and I^k_i are the previous and current registration index on kth resolution level. $Time^k_i$ is the computation time of the current registration process on the kth resolution level. $Grid^k$ is the kth resolution level grid size.

The important particles are extracted by the registration index w^k_i and registration tendency $Trend^k_i$. After sorting the particles according to their registration index, the first third are selected out as the important particles. The registration tendency $Trend^k_i$ of particle i could efficiently predict the next registration status in the next loop based on the current particle position. The parameter δ(valued from 0 to 1) is essential to determine the map updating scheme, the map would not be updated until the registration tendency decrease to a certain level. With a higher tendency index, the particle is more likely to converge into a local optimal. This property is the core criterion for map updater in next section and iteration times L selection in Section 3.C.

B. GPU based Heuristic Escape

In most ICP based registration algorithm, derivative based optimization method is used to obtain the optimal registration results. This, however, will unavoidable result in the local minima problem. Thus, the mechanism to make sure the candidate optimal solutions escape from the local minimum region is very important. In our previous work, we propose a heuristic escape scheme to handle the local minima problem, because the escape direction is based on six sampled potential directions, thus the escaping scheme is the most time consuming step in the whole registration loop. On the other hand, the escape efficiency is high related to the finite number of directions, and all potentials may suffer from the local minimal problem in the tricky situation. While the sample and weighting procedure for each potential transformation is independent, so we take a GPU enhanced parallel method to improve the escaping ability.

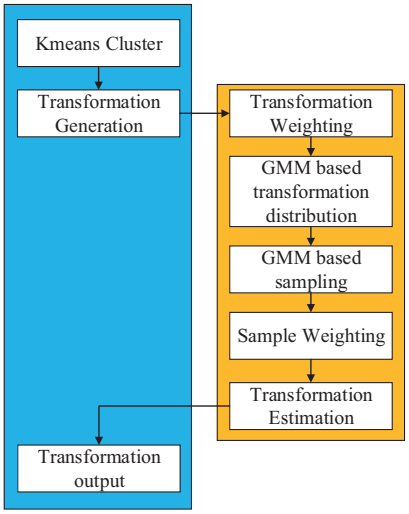

Figure 3 GPU-based Heuristic Escaping: the blue block module is applied on CPU framework and the orange block module is applied on GPU framework.

The control flow of the GPU based heuristic escaping is as shown in Figure 3. We first calculate all the Euclid distance from each point p_i in Scan pointcloud P to its corresponding point q_i in Model pointcloud Q.

$$\mathrm{dist}(p_i) = \| p_i - q_i \|, i = 1 \ldots N_p \tag{9}$$

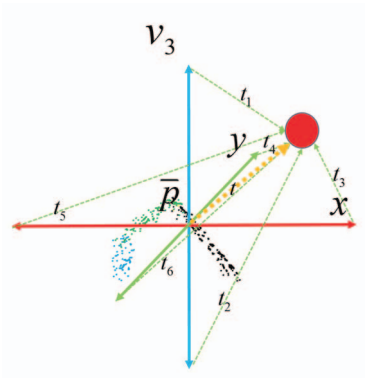

Figure 4 potential direction

According to the computed distance value of each pair of Scan Pointcloud, *Kmeans* scheme is used to divide the Scan pointcloud into several groups. The result is depicted in Figure 4, and the circled dark point sets represented the points which have the coordinate distance within given threshold. The normal vector of the extracted point cloud is estimated by the method applied in the PCL library [16]. The sex transformation is then generated based on the normal vector and the normal surface.

Instead of weighting the transformation directly, we copy the transformations from the CPU memory into the GPU memory, then six thread is allocated to imply independent ICP registration. We define the transformation from the original point to the aligned point as:

$$t_k = \begin{bmatrix} 0_{3\times3} & 1_{3\times1} \end{bmatrix} T_k^{ICP} \cdot T_k^{poten} \begin{bmatrix} 1_{3\times1} \\ 0 \end{bmatrix} \tag{10}$$

where $\{T_k^{poten}\}^6_{k=1}$ are the six potential transformation with two alone the normal vector and four on the normal surface. $T^{ICP}{}_k$ is the ICP registration result on kth potential transformation. Then a GMM model is applied on GPU by a parallel prefix to represent the transformation target $\hat{\bar{P}}_{k+1}$,

$$G(\hat{\bar{P}}_{k+1}, k) = \frac{1}{6}\sum_{i=1}^{6} \frac{\exp(-0.5(\hat{\bar{P}}_{k+1} - t_k \bar{P}_k)^T (I_{3x3} \cdot w_i^k)^{-1} (\hat{\bar{P}}_{k+1} - t_k \bar{P}_k))}{(2\pi)^{1.5} (w_i^k)^{0.5}} \tag{11}$$

$$\bar{P}_k = \frac{1}{N_s}\sum_{i=1}^{N_s} p_i^k$$

where N_s is the number of points with coordinate distance within the given value.

Based on the GMM model, a random sample step is applied on the GPU framework. A pseudo-random number generator (PRNG) is the function that yield seemingly uncorrelated numbers in sequence. Here we applied parallel counter-based pseudo-random to generate certain number of samples. Then the corresponding threads are allocated on the GPU framework, and ICP registrations are applied same as in the transformation weighting step.

$$T_{escape} = \frac{1}{\mathrm{N}_{\mathrm{sample}}} \sum_{i=1}^{N_{sample}} \theta_i \tilde{t}_i$$

$$\theta_i = \frac{\tilde{w}_i}{\sum_{i=1}^{N_{sample}} \tilde{w}_i} \tag{12}$$

where the N_{sample} is the number of samples, $\tilde{w}_i$ and $\tilde{t}_i$ is the weighting and transformation of ith sample estimated by Eq.(7) and (10). Then we transform the Scan pointcloud with the desire escape transformation, and simultaneously increase the resolution of both Scan and Model pointcloud to the primary level and continue to the Multi-Resolution scheme until the Registration Index hits the threshold value.

IV. Experiment and Results

A. Experiment Setup

Figure 4 air robot and surface robot system

To verify the performance improvement of the proposed algorithm, experiments are conducted on an air-surface heterogeneous multiple mobile robot systems at a river bank. Both robots are equipped with navigation system for pose measurement and LiDAR for environment perception, which is shown in Figure 4. The pose of each platform was estimated from the IMU (inertial measurement unit) and differential GPS, with an outputting frequency at 100 Hz. Furthermore, in

the air robot system, a Velodyne VLP-16 LiDAR system, which generates 300,000 points per seconds, is equipped, and the obtained model is called Model point cloud. While a Velodyne 32e LiDAR system is mounted on the surface robot system generating about 700,000 points per second, and the corresponding model is called Scan point cloud. We tested the registration methods in two different scenes: A slender bank with complex terrain and a triangular area with diverse elevations. Table 1 gives the details of each experiment. To verify the robustness against different resolution levels, the model point clouds were kept at the same resolution level in both experiments, but the resolution level of the scan point clouds was set to 0.5 m for the slender bank and 0.2 m for the triangular area.

Table 1. Experimental conditions.

No.	Datasets	Number of Points	Resolution
Slender bank			
ExI	Model	212,912	1 m
	Scan	40,300	0.5 m
Triangular area			
ExII	Model	212,912	1 m
	Scan	125,493	0.2 m

B. *Convergence*

Besides our proposed enhanced ICP, we also evaluated three other ICP-based methods for comparison: standard-ICP, M-ICP, and G-ICP. Figures 9 and 10 show the results for the slender bank and triangular area experiments. The red point cloud represents the model point cloud Q. The green, yellow, purple, and pink point clouds represent the registration results of the enhanced ICP, standard-ICP, M-ICP, and G-ICP, respectively. Each method was tested for both the normal initial transformation error and abrupt turn case in the experiment.

For the normal initial transformation error case, the initial translation error was randomly sampled within [±10, ±10, ±10], and the rotation error was sampled within [±20°, ±20°, ±40°]. Although all methods obtained acceptable results for the triangular area test, as shown in Figure 9b, the other methods failed to match the model point cloud for the slender bank test owing to the complexity of the terrain as shown in Figure 9a. In contrast, our proposed enhanced ICP method guaranteed correct results with a final RMS error of 1.1 m and rotation error of 1.5°. Table 2 summarizes the registration results of 40 normal initial transformation error tests on the slender bank and triangular area in Detail 2. On average, our proposed method could achieve an accurate match even with a rough initial error.

To verify the abrupt turn problem with the different ICP-based methods, we set the initial rotation error on the z-axis around 160°–220°, as shown in Figure 10. The Standard ICP, M-ICP, and G-ICP became trapped in a local minimum in both the slender bank and triangular area test. Our proposed enhanced ICP could efficiently estimate the local minimum problem by using the early warning mechanism and eventually escape with a proper transformation by using our heuristic escape scheme.

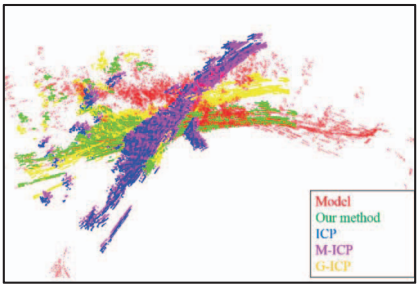

(**a**) Slender bank test

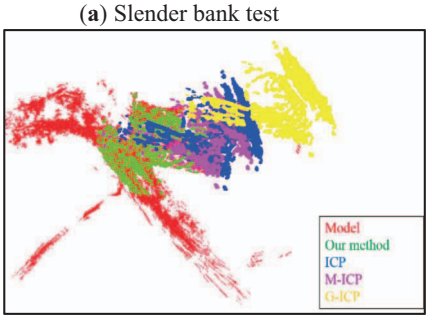

(**b**) Triangular area test

Figure 5 Matching result

Table 2. Registration results with a normal initial error.

Method	Translation e_t (m)			Rotation Error e_r (°)		
	min	μ_t	σ_t	Min	μ_r	σ_r
Slender Bank Experiment						
ICP	1.4	8.3	6.3	3.4	24.1	10.2
M-ICP	1.5	6.5	4.3	1.6	15.8	5.9
G-ICP	0.4	5.1	2.3	0.2	12.0	3.8
E-ICP	0.2	1.7	1.9	0.4	1.7	1.2
GE-ICP	0.2	1.6	1.1	0.4	1.4	1.1
Triangular area Experiment						
ICP	1.2	8.2	9.2	2.3	19.4	12.2
M-ICP	1.7	5.3	6.5	2.1	15.4	8.6
G-ICP	0.3	4.2	3.3	0.5	12.7	6.1
E-ICP	0.1	1.3	1.4	1.1	2.8	1.8
GE-ICP	0.1	1.2	0.9	0.4	1.8	1.1

*μ_t is the average translation error; σt is the variance of the translation error; μ_r is the average rotation error; and σ_t is the variance of the rotation error. The translation errors were within [±10, ±10, ±10], and the rotation errors were within [±20°, ±20°, ±40°].

C. *Running time*

Figure 6(a) presents the average registration times of the methods in both experiments with normal initial transformation errors. The proposed method was not as fast as the single standard ICP or M-ICP method. This is because of the heuristic escape scheme, which combines potential

direction estimation and G-ICP to escape from the local minimum. On average, our proposed method reduced the registration time by 30% compared to G-ICP while guaranteeing registration accuracy at the same time. For the abrupt turn case, we only evaluated the relation between the RMS error and registration time of our proposed method. As shown in Figure 6(b), the registration time for the abrupt case was closely related to the heuristic escape time, as given in Figure 8. A larger initial transformation error increased the heuristic escape time, which also increased the computation time.

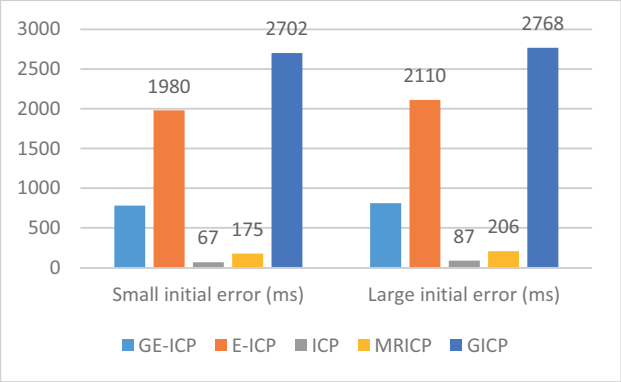

Figure 6. Time cost analysis: (a) in both Slender Bank test and Triangle Area test, our method could make the alignment around 2 seconds, faster than the generalized ICP but slower than the standard-ICP method and multi-resolution ICP method because of the heuristic escape scheme; (b) the registration time is highly related to RMS error because of the heuristic escape scheme.

V. CONCLUSIONS

In this paper, the problem of fast and accurate registration of large scale 3D environmental model in the applications of heterogeneous mobile robot sensing information fusion. A new registration algorithm is proposed based on the coarse-to-fine multi-resolution scheme and a new introduced heuristic local minimum escape method. Experiments of the new proposed algorithm is conducted with respect to the environmental point cloud information fusion of an air robot and a surface robot. The results are compared to that of some other registration algorithms (standard ICP, Multi-Resolution ICP and Generalized-ICP) and show that the new proposed algorithm is insensitive to the initial errors and present higher precision.

REFERENCES

[1] P. Besl and N. McKay, "A Method for Registration of 3-D Shapes," *IEEE Transactions on Pattern Analysis and Machine Intelligence*, vol. 14. pp. 239–256, 1992.

[2] S. Y. Park and M. Subbarao, "An accurate and fast point-to-plane registration technique," *Pattern Recognit. Lett.*, vol. 24, no. 16, pp. 2967–2976, 2003.

[3] a Segal, D. Haehnel, and S. Thrun, "Generalized-ICP," *Robot. Sci. Syst.*, 2009.

[4] T. Jost and H. Hugli, "A multi-resolution ICP with heuristic closest point search for fast and robust 3D registration of range images," *Fourth Int. Conf. 3-D Digit. Imaging Model. 2003. 3DIM 2003. Proceedings.*, no. 3dim, pp. 0–6, 2003.

[5] J. Yang, H. Li, and Y. Jia, "Go-ICP: Solving 3D Registration Efficiently and Globally Optimally," *2013 IEEE Int. Conf. Comput. Vis.*, pp. 1457–1464, 2013.

[6] J. Han, P. Yin, Y. He, and F. Gu, "Enhanced ICP for the Registration of Large-Scale 3D Environment Models : An Experimental Study," pp. 1–15, 2016.

[7] M. Grabner, T. Pock, T. Gross, and B. Kainz, "Automatic Differentiation for GPU-Accelerated 2D / 3D Registration," *Adv. Autom. Differ.*, vol. 64, pp. 259–269, 2008.

[8] D. Qiu, S. May, and a. N\"uchter, "GPU-accelerated nearest neighbor search for 3D registration," *Comput. Vis. Syst.*, vol. 5815, pp. 194–203, 2009.

[9] C. Bodensteiner and M. Arens, "Real-time 2D Video / 3D LiDAR Registration," *Int. Conf. Pattern Recognit.*, no. Icpr, pp. 2206–2209, 2012.

[10] M. Liu, F. Pomerleau, F. Colas, and R. Siegwart, "Normal estimation for pointcloud using GPU based sparse tensor voting," *2012 IEEE Int. Conf. Robot. Biomimetics, ROBIO 2012 - Conf. Dig.*, pp. 91–96, 2012.

[11] T. Jost and H. Hugli, "A multi-resolution scheme ICP algorithm for fast shape registration," *Proceedings. First Int. Symp. 3D Data Process. Vis. Transm.*, pp. 2000–2003, 2002.

[12] P. Besl and N. McKay, "A Method for Registration of 3-D Shapes," *IEEE Trans. Pattern Anal. Mach. Intell.*, vol. 14, no. 2, pp. 239–256, 1992.

[13] M. Greenspan and M. Yurick, "Approximate K-D Tree Search for Efficient ICP," *3-D Digit. Imaging Model. 2003. 3DIM 2003. Proceedings. Fourth Int. Conf.*, pp. 442–448, 2003.

[14] F. Pomerleau, F. Colas, R. Siegwart, and S. Magnenat, "Comparing ICP variants on real-world data sets," *Auton. Robots*, vol. 34, no. 3, pp. 133–148, 2013.

[15] C. Nvidia, "NVIDIA CUDA C Programming Guide," *Changes*, no. October, p. 173, 2011.

[16] R. B. Rusu, N. Blodow, and M. Beetz, "Fast Point Feature Histograms (FPFH) for 3D registration," *2009 IEEE Int. Conf. Robot. Autom.*, 2009.